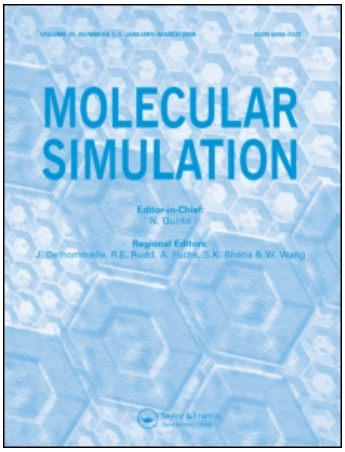

Molecular Simulation
Publication details, including instructions for authors and subscription information:
http://www.informaworld.com/smpp/title~content=t713644482

Molecular Dynamics Simulations for Metallic Nanosystems

A. Hasmy[a]; P. A. Serena[ab]; E. Medina[a]
[a] Laboratorio de Física Estadística de Sistemas Desordenados, Centro de Física, IVIC, Caracas, Venezuela [b] Consejo Superior de Investigaciones Científicas, Instituto de Ciencias de Materiales de Madrid, Madrid, Spain

Online publication date: 26 October 2010

To cite this Article Hasmy, A. , Serena, P. A. and Medina, E.(2003) 'Molecular Dynamics Simulations for Metallic Nanosystems', Molecular Simulation, 29: 6, 427 — 435
To link to this Article: DOI: 10.1080/0892702031000148744
URL: http://dx.doi.org/10.1080/0892702031000148744

Molecular Simulation, VOL. 29 (6–7), June 2003, pp. 427–435

Molecular Dynamics Simulations for Metallic Nanosystems

A. HASMY[a,*], P.A. SERENA[a,b] and E. MEDINA[a]

[a]*Laboratorio de Física Estadística de Sistemas Desordenados, Centro de Física, IVIC, Apartado 21827, Caracas 1020A, Venezuela;* [b]*Instituto de Ciencias de Materiales de Madrid, Consejo Superior de Investigaciones Científicas, Cantoblanco, 28049 Madrid, Spain*

(Received November 2002; In final form December 2002)

Nanotechnology is a crucial field for future scientific development where many different disciplines meet. Computational modelization of nanometer-sized structures is a key issue in this development because (i) it allows a considerable saving of resources and costly experimental setups intended to fabricate nanometric test devices and (ii) nowadays the study of nanometric sized systems is feasible with thoroughly designed computational codes and relatively low cost computational resources. This article describes how molecular dynamics simulations, in combination with potentials obtained in the framework of the embedded atom method, are able to describe the properties of two systems of interest for the development of future nanoelectronic devices: metallic nanowires and metallic nanofilms. Our results show that nanowire stretching results in a series of well-defined geometric structures (shells) and that thin films experiment a crystallographic phase transition for a decreasing number of layers. In both cases, good agreement with experiments is found.

Keywords: Nanotechnology; Embedded atom method; Molecular dynamics simulations; Ionic shells

INTRODUCTION

Nanotechnology and its many different branches have become a key point for future development in physics, chemistry, biology and materials science. Among different subjects, the study of the structure of nanoscale sized systems as well as their interactions with external fields represents one of the major interests of the scientific community. In particular, the physics of electronic transport through structures formed by only a few hundred atoms (nanowires or nanocontacts) is crucial in future nanoelectronics developments. Such nanostructures will act as links among logical elements in electronic devices, fabricated with an unprecedented scale of integration [1]. Furthermore, these objects present mesoscopic properties providing them with additional value for other applications. Additional challenges correspond to device design at the nanoscale, which is also experimenting important developments. As one attempts to give suitable shapes to smaller and smaller amount of matter in order to fabricate specific devices with well defined volume limitations, one meets an intrinsic limit to the design given by the stability of the resulting nanostructure [2,3].

At the nanoscale, experiments are difficult due to high costs and instrumental technological limitations. In this direction, computer simulations have become an alternative approach to many areas of condensed matter and material science [4]. Then it seems an appropriate methodology to assess physical phenomena, and understand different problems associated with the fabrication of device prototypes in industry. In this sense, nanotechnology appears as a ideal field where computational tools, based on our knowledge of Quantum Mechanics, will be useful with few restrictions.

Electronic structure calculations based on density functional theory [5] and computer simulations based on Molecular Dynamics (MD) have greatly contributed to the understanding of equilibrium and non-equilibrium properties of condensed-matter systems [4,6]. Although the accuracy of this kind of calculation is usually satisfactory, they are computationally so demanding that only few atoms can be treated routinely. Traditional electronic structure algorithms calculate eigenstates associated with discrete energy levels. A disadvantage of this approach is that it leads to a diagonalization problem that has a cubic scaling with respect to the size of the Hamiltonian matrix, i.e. with

*Corresponding author. E-mail: anwar@ivic.ve

ISSN 0892-7022 print/ISSN 1029-0435 online © 2003 Taylor & Francis Ltd
DOI: 10.1080/0892702031000148744

respect to the number of basis functions N_b. Iterative diagonalization schemes, preconditioned conjugate-gradient minimizations, and the Car–Parrinello method for MD simulations have been a substantial algorithmic advance providing an improvement in the scaling of computational time [7]. Using such methods, it is no longer proportional to the cube of the number of basis functions, but grows only like $N_b \log(N_b)$ if plane waves are used as a basis set. Nevertheless, this method still has a cubic scaling with respect to the number of atoms N, which comes from the orthogonality requirement of the wave functions. The reason why this orthogonalization step scales cubically can be easily understood. As the system grows, each wave function extends over a larger volume and therefore has to be represented by a larger basis set, resulting in a vector with many more components. At the same time, there are more such wave functions and each wave function has to be orthogonalized to all the others. Thus, there are three factors that grow linearly, resulting in the postulated cubic behavior. Therefore, by enlarging the system one rapidly reaches the limits of the most powerful computers. Other problems associated with approaches like the Car–Parrinello method arise from the fact that involved approximations (i.e. the assumption of the coupling between electronic and ionic motions) requires very short time intervals. Furthermore, for the simulation of metallic systems the Car–Parrinello methodology fails because there is no consistency of this approximations with the typical electron delocalization in metals [8].

Several empirical methods have been proposed in the past [4]. They are based on a parameterization of the interaction potential, typically obtained by fitting bulk and surface properties. This kind of method neglects modelization of the electronic structure, then the computational time involved is radically smaller than that of the quantum computational methods. The most known effort on this direction is the development of optimized pairwise interaction potentials. However, this approach also fails when describing metallic systems because a volume dependent term is lacking; a requirement of metals in order to take into account electronic delocalization. Many methods have been proposed which incorporate the corresponding multibody contribution. All of them based on the effect of the electronic density which acts on each atom.

The most popular empirical method that includes multibody contributions corresponds to the embedded atom method (EAM) [9]. Even though this method has enjoyed a great deal of success in accounting for many of the bulk properties of single crystals [9,10] and alloys [11], the melting transition [11,12], vacancy formation [13], the description of liquid metals [14] as well many surface properties, its applicability to nanoscale science has not been fully demonstrated. One of the reasons is that embedding functions (those containing the basic information describing the interactions between atoms and the surrounding electronic sea) are generally obtained by fitting many established bulk and surfaces properties, but not that corresponding to the system at nanoscale. That is, it is not clear than those embedding functions used to describe bulk systems are transferable to low dimensional problems. Recently, some researchers have proposed embedding functions able not only to recover macroscopic properties but also microscopic ones, including the distance between an atomic dimer [15].

In this paper, we describe a combination of MD techniques with EAM, for the simulation of metallic nanosystems. We review two examples of MD simulations that demand little time and describes quite well the corresponding experiments. Our approach allows predictions for larger scale atomic systems with a relatively small cost, as compared to experiments. First, we will present a statistical study of the formation of metallic nanocontacts, and will provide evidence of preferable atomic configurations at the nanocontact necks. Finally, we will present simulations of a large variety of metallic nanofilms, and will show that film thickness induces a generic structural transition in such systems. Short reports of some of these results have been published elsewhere [16,17].

MD SIMULATIONS WITH EAM

MD is a widely used method for studying many-particle systems [4]. Such technique has been combined with the EAM, which describes the interaction potential among atoms. EAM includes in a realistic way the interaction of an atom with the electronic cloud where it is immersed. This is a semiempirical method for calculating, in an efficient manner, the energy of a metallic system including many-body cohesive effects [9]. Under this approach, the structural energy of the metallic system is expressed as a combination of two terms, a pair repulsive term $\phi(R_{ij})$ and an energy embedding function $F(\rho_i)$:

$$E = \sum_i F(\rho_i) + \frac{1}{2}\sum_{i \neq j} \phi(R_{ij}) \tag{1a}$$

with:

$$\phi(R_{ij}) = Z^2(R_{ij})/R_{ij} \tag{1b}$$

where the function $Z(R_{ij})$ corresponds to an effective charge as a function of the interatomic distance R_{ij}. The other term is the energy function $F(\rho_i)$, which

embeds each atom i in the local electron density ρ_i:

$$\rho_i = \sum_j k_j(R_{ij}) \tag{2}$$

where k_j is the electron density of the atom j provided by the other atoms. The forces are obtained by a simple differentiation of the potential energy with respect the distance between atoms.

In the examples that we will present here, for the formation of metallic nanocontacts we implemented a constant energy methodology, which implies an average as in the microcanonical ensemble. For the example where nanofilms are studied, we required volume fluctuations. For this, an additional equation of motion for the box containing the system have been considered, which has been coupled with the equation of motion of particles in order to preserve constant pressure [18]. In all simulations we present here, the temperature has been controlled using a simple scaling velocities procedure [18].

IONIC SHELL AND SUBSHELL STRUCTURES IN NANOWIRES

Background

Metallic contacts have been used for the study of electronic transport in nanowires. From an experimental point of view, such study has been carried out with scanning tunneling microscopy (STM) [19–23], the Mechanically Controllable Break Junction method [24–26] and even between two plain macroscopic wires [27]. The nanocontact is stretched with a simultaneous application of a bias voltage. Conductance jumps appear during the nanowire breaking process correspond to changes of the transmission probability of the propagating modes.

Since every single contact-breaking experiment has its own conductance evolution, transport in these systems has been evaluated statistically, building conductance histograms (CH) to analyze the electrical behavior of nanocontacts. In general, CH show a well-defined peaked structure, with higher conductance probabilities close to integer values of G_0 (the quantum conductance). Although CH have become a standard tool to study metallic nanocontacts, there is no solid theoretical background justifying their use. Any realistic interpretation of CH should take into account the strong coupling between electronic and mechanical properties [28], since conductance and force jumps are correlated through crystalline rearrangements inside the nanocontact as predicted by MD simulations [29]. Therefore, CH give information of the conductance, while the measured histogram weights are related to the stability of a given conductance situation.

For monovalent systems like gold it has been demonstrated that each quantum conductance G_0 ($= 2e^2/h$) corresponds to the contribution of the transport of one atom at the neck [54]. For other species with higher chemical valence, it has been shown [30,31] that a monoatomic Al contact conducts through 3 available channels, with a total conductance of approximately 1. By comparing Al experimental CH and MD simulations, a previous work [32] confirms the close correspondence between conductance and the number of atoms in the wire cross-section.

Simulation of Nanocontact Rupture

For the MD simulation of nanocontact formation, we considered a parallelepiped supercell containing atoms ordered according to a fcc crystallographic structure, with the respective lattice constant of the bulk metal system. The atoms were initially distributed in 18 layers (of 200 atoms each) perpendicular to the (111) direction, which is the more favorable orientation as we will see in the next section. The (111) direction (the z axis in our simulation) corresponds to that in which the contact will be elongated until breaking. In this work we address such a study for Au and Al nanocontacts.

Each single MD simulation consists of three stages. First, we relax the initially ordered system for 2000 iterations, imposing periodic boundary conditions (PBC) in the x and y directions of the sample. The time interval per iteration step in all our simulations is $dt = 10^{-14}$ s. During the equilibration stage the system undergoes a relaxation characterized by a contraction along the z axis. In the final thermally equilibrated structure, two bi-layer slabs are defined at the top and bottom of the supercell. All atomic positions inside these slabs are frozen during subsequent MD stages, defining the bulk support of the nanocontact during the breaking process. In a second stage, the system is again thermally equilibrated during 3000 iterations, but now PBC are preserved only in the x and y directions of the frozen slabs. The other atoms, defining a free nanowire, evolve to reach a new equilibrium configuration. The third stage corresponds to the nanowire stretching, separating both supporting frozen slabs at a constant velocity of 2×10^{-4} Å per iteration step. Such a choice for the stretching velocity ensures a quasi-stationary rupture as previously demonstrated [33,34]. The evolution of atomic positions during the elongation allows us to know the changes of the nanocontact geometry, and evaluate the time evolution of the minimum cross-section S_N (in units of numbers of atoms) as in Refs. [35,36]. This magnitude determines the effective number of atoms located at the region where the nanowire cross-section presents its minimum value along the nanowire, being closely

related to the nanowire conductance. For the interaction potential energy, we used the state of the art of embedding functions suggested in Refs. [15,37] for Al and Au, respectively. For the Au case, the improvement over previous embedding functions reported in the literature is related to their ability in recovering experimental surface energies [37]. For Al, in addition to the above macroscopic ability, the embedding functions also fit microscopic properties as, for instance, the bonding length of Al dimer obtained from *ab initio* calculations [15].

By computing the total neck area cross-section A_n from:

$$A_n = S_N a_o \tag{3}$$

where a_o is the bulk atomic cross-section, one can estimate the neck radius R by calculating $(A_n/\pi)^{1/2}$. A first approximation for the conductance of nanocontacts is obtained by a simple relation to their cross section through the Sharvin semiclassical formula [38]:

$$\left(\frac{G}{G_0}\right) = \left(\frac{k_F R}{2}\right)^2 \left(1 - \frac{2}{k_F R} + \cdots\right) \tag{4}$$

where k_F is the Fermi wave vector. Within these approximations, an Aluminum contact of one and two atoms have $g = 0.92$ and 1.84 (being $g = G/G_0$ the dimensionless conductance), respectively, which are values close to those observed in experiments. In this section we considered only room temperature (300 K).

Shell and Subshell Structure

An example of nanocontact stretching is depicted in Fig. 1(a). In Fig. 1(b) we show the evolution of the minimum cross-section S_N as a function of the nanocontact elongation Δd for four different realizations. By accumulating a large number of traces and applying Eq. (4) we construct CH $H(G)$. The number of single nanowire breaking realizations N_s considered is such that the obtained relative histogram peak structures are unchanged under further averaging (see Fig. 1(c)). In our calculations, we found that $N_s = 100$ provides a reliable $H(G)$ curve. We have also tested that minimum cross-sections histograms do not depend on the initial nanowire diameters. In particular, we have found no differences in the peak structure of $H(G)$ at low conductance values when considering initial cross-sections of the wire containing 54 atoms [16] and 200 atoms (this work). This evidences the non-dependence of histogram on the considered range of sizes we have analyzed. Figure 2 shows the simulated CH for Al and Au with a larger conductance ($0 \leq g \leq 175$) window sizes.

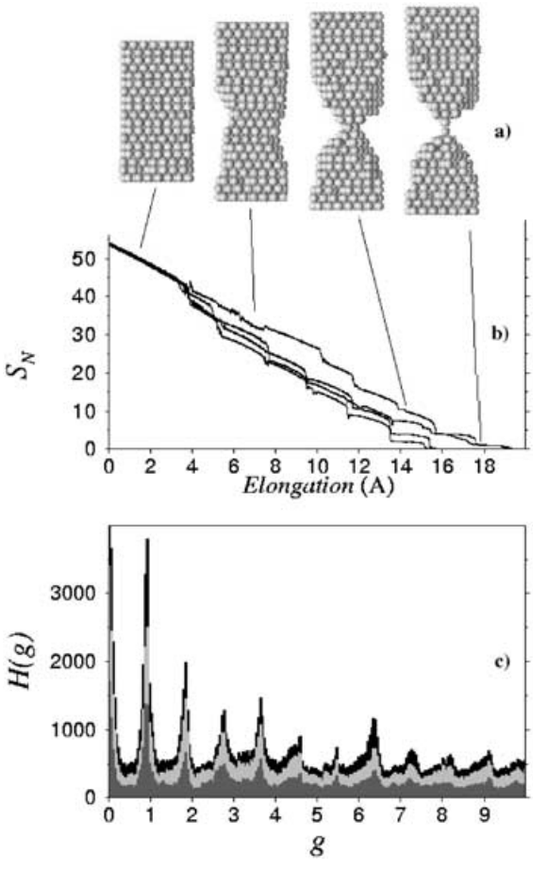

FIGURE 1 (a) Typical nanocontact configurations during the elongation of the sample. (b) Minimum cross-section S_N evolution for four Al nanowires. Each nanowire evolves in a different way due to the initial random choice for atomic velocities (according to Maxwell distribution). The stretching direction is parallel to the (111) direction, and the arrows indicate the corresponding S_N for each configuration. (c) Simulated CH $H(g)$. Dark gray, gray and black curves correspond to histograms obtained with different number of realizations (35, 70 and 100, respectively).

As for clusters, the shell structure can be revealed by demonstrating a linear relation between wire radius and peak number of the oscillating thermodynamic potential determining the stability of the structure [39,40]. This in turn leads to the probability of occurrence of the particular geometric configuration. In nanowires this is related to the predominance of a particular wire cross section, which can directly monitored by the conductance [41,42] because $(G/G_0)^{1/2} \propto R$ as can be seen from Eq. 4 (apart from small corrections from the perimeter contribution). Therefore, a linear relation of such a quantity versus the peak number in the Au and Al histograms of Fig. 2 indicates the existence of shells. Figure 3 shows $(G/G_0)^{1/2}$ versus the conductance peak number for Au and Al. The data points first rise in a non-linear fashion and then settle onto a linear behavior of slope 0.21 ± 0.02 (see open symbols). Also indicated in the figure is the expected slope for electronic shells, according to jellium theories, of

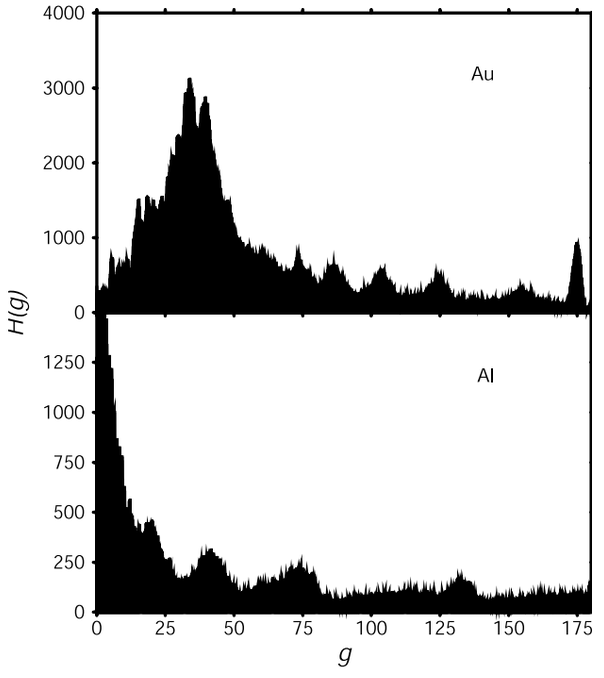

FIGURE 2 CH for Au and Al at room temperature.

$\sim$0.59 as reported in Refs. [41,42]. No indication of electronic shells is then evident from our results since slope differences are beyond the simulated error. The initial non-linear behavior seems to follow in part from the successive occupation of individual quantum modes leading to regular conductance quantization. The order in this first sequence of peaks is then $\propto R^{1/2}$ (G and the peak number are linearly related) emulating the initial structure. Comparison between our numerical results and experimental data [43] with a similar procedure of Yanson *et al.* [41,42] provides evidence of good agreement. However, it should be pointed out that in contrast to the Al case [32], for Au the EAM potentials used are unable to emulate the stability of Au nanocontact of only few atoms at the neck, i.e. the experimental relative amplitudes of the peaks at low conductance values are not recovered, perhaps due to relativistic effects and the electronic energy corrections unaccounted for with the EAM.

We are thus led to the analysis in terms of ionic shells. The inset of Fig. 3 shows two proposed candidate structures for fcc metal nanowires. The first one has an hexagonal cross section with an axis oriented in the (0 1 1) direction, and six equal area facets, four of them hexagonally packed, while the remaining two facets are perpendicular to the (1 0 0) direction. This is the structure that would be derived from a Wulff type construction. The second candidate structure was derived from Refs. [44,45] and is octagonal, also with an axis in the [0 1 1] direction with facets of exposed area fractions β_{ijk}: $\beta_{111} = 0.55$, $\beta_{100} = 0.25$ and $\beta_{110} = 0.20$. Such a structure takes into account both surface and edge energies.

Growing the cross sections of the proposed wire structure by complete layers of atoms, increases the wire radii deterministically and results in an increase of the number of propagating electron channels. Using Eq. (4), dropping the perimeter correction, one can compute the conductance g as a function of the number of complete crystalline layers m. The derivative of such expression leads to a relation for the slope:

$$\alpha_1 = d(g^{1/2})/dm = 3^{5/6}\pi^{1/6}/2^{13/12} \qquad (5)$$

which is approximately equal to 1.427 [46]. Such a slope is depicted in Fig. 3, and is clearly too high to explain the results. Nevertheless, if facets are filled individually, as previously discussed in Al clusters, and suggested by Yanson *et al.*, the slope decreases six-fold, i.e. $\alpha_1/6 \sim 0.24$ in closer agreement with the data.

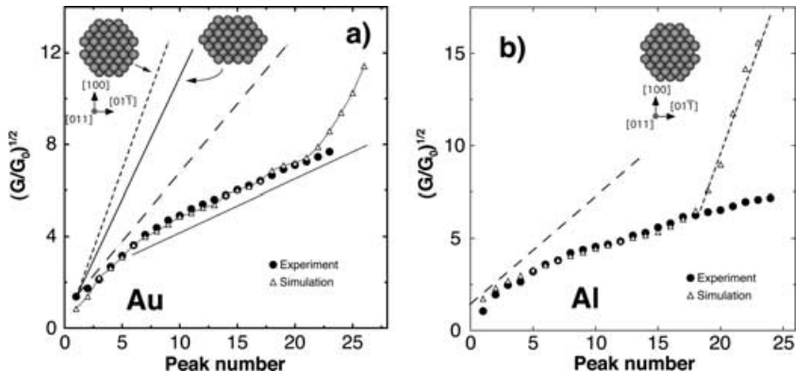

FIGURE 3 $(G/G_0)^{1/2}$ versus the peak number for Au (a) and Al (b), as obtained from simulations (open symbols). The black symbols correspond to experimental data of Ref. [43]. The different lines illustrate the expected behavior of $(G/G_0)^{1/2}$ for different modes of nanowire growth: octagonal shells (short dashed line), hexagonal shells (thick solid line), electronic shells (long dashed line) and octagonal facets (thin solid line). The inset illustrate the candidate crystalline structures proposed for the section of the wire corresponding to the full ionic shell slopes (see text).

The second proposed cross section, leads to the slope $\alpha_2 \sim 1.844$. Dividing by eight facets yields $\alpha_2/8 \sim = 0.23$, approaching slightly better the measured slope. Although there are small differences in the slopes, probably related to the simple first-order Sharvin conductance formula used, the second proposed crystalline section approaches the measured value within the error bars.

An advantage of the simulation is that we can go more easily to larger conductance values than experiments. Nevertheless, for large diameter wires the detailed peak structure observed at intermediate conductance values (ionic subshell signature) is unresolved in simulations as can be seen in Fig. 2. In other words, at high g values the broader maxima obscure details of the peak structure corresponding to subshells observed at intermediate g, but evidences complete ionic shells. In fact, the high slope at large conductance values agrees well with that expected for complete shells for the octagonal candidate crystalline structure.

STRUCTURAL TRANSITION IN METAL NANOFILMS

Background

It is well established that many (0 0 1)-oriented surfaces of fcc metals on a substrate reconstruct to a contracted, quasi-hexagonal, close packed layer [37,47,48,49]. The driving force for the reconstruction is a reduction of the surface energy enough to compensate for the ensuing mismatch strain. Similar reconstructions apply to the (0 0 1) facet of small gold clusters [50], and the hexagonal surface reconstruction of gold nanowires [2]. Nevertheless, surface reconstruction on a substrate in fcc metals is by no means spontaneous and favored. In fact, it is observed that stress overcomes the substrate resistance to produce spontaneous reconstructions only in 5*d* metals (Ir, Pt, Au), whereas in 4*d* metals (Rh, Pd, Ag) external stress must be applied [47]. Reconstruction can also be induced by increasing temperature as in heterogeneous adsorbate-substrate systems [51].

For free standing or suspended metallic films, surface stress should become increasingly comparable to the remaining bulk forces as film width shrinks. Recently, it has been suggested that such a tendency drives striking filmwide reconstructions in gold nanofilms [52]. The initial gold (0 0 1) oriented film is made by vacuum deposition, and a local thinning process is performed by electron beam irradiation. When the irradiated region becomes very thin, 2–3 nm, the film spontaneously transforms into the (1 1 1) orientation. Our scope is to reproduce with simulation such phenomenon as well as predict if it occurs in other fcc metals.

Simulation of Nanofilms

We performed MD simulations for fcc metal nanofilms, taking into account the (0 0 1) oriented border constraints, due to the bulk unthinned film, in the real experimental situation [52]. The implemented method for pressure control and isotropic volume fluctuations corresponds to a modified Andersen scheme as explained in Ref. [18].

As the initial configuration, we considered a cylindrical geometry where the external annular region has an fcc crystalline structure with a (0 0 1) surface orientation perpendicular to the cylinder axis. Within this annulus we place a cylindrical test film with a given number of layers. The thermal energy of atoms in the annulus is ignored (i.e. these atoms are frozen), but they can move with the whole sample due to the kinetic volume energy as required by the constant pressure constraint. The isotropic volume contraction is limited only by the core–core repulsion between annular frozen atoms at the borders of the nanofilm. The integration of equation of motions is done by a fourth order predictor-corrector method with a 10^{-15} s time step. As in the preceding section, we considered the same state of the art of embedding functions [15,37,48].

The initial metal film diameter considered is approximately 5 nm (corresponding to the non-frozen atoms region), much larger than their thickness 1.4–3.5 nm. At a given temperature, the system is allowed to relax for 2×10^5 time steps (2^{-10} s). This time is enough to reach a quasi-equilibrium state where energy fluctuates around an average value.

Nanofilm Transition

In Fig. 4 we present a cut of different relaxed configurations for Au systems with an initial number of layers $N_l = 20$, 16 and 12 and room temperature. Gray (top layer) and white (secondary layer) atoms correspond to free atoms. Darker atoms in the annulus have a fixed lattice arrangement only subject to contraction controlled by the isobaric MD. The figure clearly shows: (i) (left panel) the absence of both surface or bulk reconstruction, with only a slight mismatch between the film and the annulus, (ii) surface reconstruction (middle panel) to an hexagonal arrangement, while the bulk of the film still retains its (0 0 1) orientation with some relaxation and (iii) surface and bulk (filmwide) reconstruction appearing at the center of the sample film that relaxes to a (1 1 1) (layer by layer) orientation, as observed in experiments.

A mismatch transition region is also seen in Fig. 4, accommodating annular and bulk film lattice parameters. Surprisingly, for a similar diameter and $N_l = 8$ ($\sim$1.45 nm, the minimum critical thickness

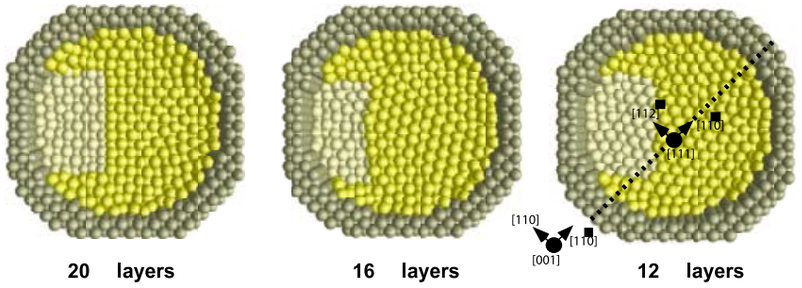

FIGURE 4 Top view of typical Au nanofilms configurations after equilibration at room temperature. Left, center and right panels correspond to film of initially 20, 16 and 12 layers. Dark spheres at the borders correspond to frozen (0 0 1) atoms. The film atoms shown as gold and white (see online edition) correspond to the top and secondary layer, respectively. The (0 0 1) oriented border annulus and (1 1 1) oriented films are rotated relatively 35° around the [$\bar{1}$ 1 0] axis bringing the [1 1 0] direction of the (0 0 1) film parallel to the [1 1 $\bar{2}$] direction of the (1 1 1) transformed film, as reported in experiments.

accomplished in experiments) a small thermal activation energy ($\sim$100 K) is required to achieve the transformation. Below such an energy barrier we observe the formation of large dislocations crossing the sample. We also observed that on increasing the film diameter and preserving its thickness, results in reduction of the required thermal activation energy for transformation. The existence of a finite energy barrier cannot be ruled out by the experiments, where local temperature was only estimated as an upper bound (429 K), so thermal effects were excluded to within a few hundred Kelvin.

We also implemented simulated thinning processes for other relevant metallic samples such as Al, Ag, Ni and Pt. In all cases we were able to obtain the film transformation from (0 0 1) to (1 1 1). However, we evidenced that the required thermal activation energy strongly depends on the metal species. For samples of initial $N_l = 8$ and similar diameters as above, the transition occurs at approximately $T = 35 \pm 10$ K for Ag, 150 ± 25 K for Al, 600 ± 30 K for Ni and 60 ± 20 K for Pt.

A robust confirmation of the predictive nature of the simulation is the quantitative verification of the relative rotation between the fixed (0 0 1) boundary and the transformed (1 1 1) film. As reported in experiments, films (frozen and thinned) are rotated 35° around the [$\bar{1}$ 1 0] with respect to one another. This brings the [1 1 $\bar{2}$] axis of the (1 1 1) parallel to the [1 1 0] direction. Such orientations are depicted in the right panel of Fig. 4 and are most likely related to a reduction of perimeter mismatch energy. The perimeter stresses, relaxed by a gradual interface between the transformed film and the fixed annulus, turn out only to decrease the energy barrier between the two crystalline configurations. This can be understood in terms of the nucleation of newly oriented material (see Fig. 4) at the center of the films to an extension such that it can meet the fixed boundary conditions [52].

Transformed film samples always contracted by approximately 5% with respect to their bulk counterparts. As in nanofilm experiments, we observe a distributions of lattice spacings, but with a better defined average behavior. We recall that a contraction of 5% is consistent with a 5×20 surface reconstruction. This result supports the fact that the film transformation is initiated by the surface reconstructions, i.e. resulting surface forces drive the change of the original structure inside the film.

CONCLUSION

We described molecular dynamics technique combined with EAM for the simulations of metallic nanosystems. In particular, we focused our research onto two different problems. First, we addressed the study of the formation of stable metallic nanonecks, finding that there is evidence of preferably atomic configurations related to the completion of shells or subshells (facets). These preferred configurations are also seen during the nanocontact breakage in good agreement with experiments where conductance histograms of breaking nanocontacts have been collected. A second study has been done to determine how thickness induces structural transition from orientation (0 0 1) to (1 1 1) in metallic nanofilms, as observed in Au nanofilms experiments. The simulations also indicate that this structural transformation in nanofilms is generic in fcc metals. In both cases (nanocontacts and nanofilms), the experimental and computational approaches remarkably agree, confirming the high quality of the embedding functions we used.

The agreement between experiments and simulations suggests that the MD-EAM scheme we have used provides a powerful tool for the study of metallic nanosystems formed by few atoms where effects due to low dimensionality are crucial. The validity of this procedure depends on the reliability and quality of the embedding functions characterizing the interatomic interaction. At this point, we

must recall that more work should be done to fully determine the EAM potential of Au since the minimum cross-section histograms we have obtained do not reflect the high stability of nanocontacts formed by one or two atoms, where chain-like structures could appear [53].

Acknowledgements

We would like to acknowledge Cecalcula (Venezuela) for computer facilities. This work has been partially supported by the CSIC-IVIC researchers exchange program and the Spanish DGICyT (MEC) through Projects BFM2000-1470-C02-01 and MAT2000-0033-P4-03.

References

[1] Serena, P.A., García, N., eds, (1997) *Nanowires* NATO ASI Series E (Kluwer, Dordrecht) Vol. **340**.
[2] Kondo, Y. and Takayanagi, K. (1997) "Gold nanobridge stabilized by surface structure", *Phys. Rev. Lett.* **79**, 3455–3458.
[3] Tosatti, E. and Prestipino, S. (2000) "Weird gold nanowires", *Science* **289**, 561.
[4] Rapaport, D.C. (1997) *The art of Molecular Dynamics Simulations* (John Wiley and Sons, New York).
[5] Payne, M., Teter, M., Allan, D., Arias, T. and Joannopoulos, J. (1992) "Iterative minimization technique for *ab initio* total-energy calculations: molecular dynamics and conjugate gradients", *Rev. Mod. Phys.* **64**, 1045.
[6] Oguchi, T. and Sasaki, T. (1991) "Density-functional molecular-dynamics method", *Prog. Theor. Phys.* Suppl. **103**, 93.
[7] Car, R. and Parrinello, M. (1985) "Unified approach for molecular dynamics and density-functional theory", *Phys. Rev. Lett.* **55**, 2471–2474.
[8] Pandey, A.C., Williams, A.R. and Janak, J.F. (1995) "Localized orbital theory of electronic structure: a simple application", *Phys. Rev. B* **52**, 14415–14420.
[9] Daw, M.S., Foiles, S.M. and Baskes, M.I. (1993) "The Embedded Atom Method: a review of theory and applications", *Mater. Sci. Rep.* **9**, 251–310.
[10] Foiles, S.M., Baskes, M.I. and Daw, M.S. (1986) "Embedded-atom-method functions for the fcc metals Cu, Ag, Au, Ni, Pd, Pt, and their alloys", *Phys. Rev. B* **33**, 7983–7991.
[11] Richardson, C.F. and Clancy, P. (1992) "Contribution of thermal conductivity to the crystall-regrowth velocity of embedded-atom-method-modeled metals and metal alloys", *Phys. Rev. B* **45**, 12260–12268.
[12] Chen, E.T., Barnett, R.N. and Landman, U. (1989) "Crystal-melt and melt-vapor interfaces of nickel", *Phys. Rev. B* **40**, 924–932.
[13] Adams, J.B., Foiles, S.M. and Wolfer, W.G. (1989) "Self-diffusion and impurity diffusion of fcc metals using the five-frequency model and the Embedded-Atom-Method", *J. Mater. Res.* **4**, 102–111.
[14] Foiles, S.M. (1985) "Application of embedded-atom method to liquid transition metals", *Phys. Rev. B* **32**, 3409–3415.
[15] Mishin, Y., Farkas, D., Mehl, M.J. and Papaconstantopoulos, D.A. (1999) "Interatomic potentials for monoatomic metals from experimental data and *ab initio* calculations", *Phys. Rev. B* **59**, 3393–3407.
[16] Hasmy, A., Medina, E. and Serena, P.A. (2001) "From favorable atomic configurations to supershell structure: a new interpretation of conductance histograms", *Phys. Rev. Lett.* **86**, 5574–5577.
[17] Hasmy, A. and Medina, E. (2002) "Thickness induced structural transitions in suspended fcc metal nanofilms", *Phys. Rev. Lett.* **88**, 096103.
[18] Heermann, D.W. (1990) *Computer Simulation Methods* (Springer-Verlag, Berlin).
[19] Pascual, J.I., Méndez, J., Gómez-Herrero, J., Baró, A.M., García, N. and Binh, V.T. (1993) "Quantum contact in gold nanostructures by scanning tunneling microscopy", *Phys. Rev. Lett.* **71**, 1852–1855.
[20] AgraÏt, N., Rodrigo, J.G. and Vieira, S. (1993) "Conductance steps and quantization in atomic-size contacts", *Phys. Rev. B* **47**, 12345.
[21] Olesen, L., Laegsgaard, E., Stensgaard, I., Besenbacher, F., Schiotz, J., Stoltze, P., Jacobsen, K.W. and Norskov, J.K. (1994) "Quantized conductance in an atom-sized point contact", *Phys. Rev. Lett.* **72**, 2251–2254.
[22] Olesen, L., Laegsgaard, E., Stensgaard, I., Besenbacher, F., Schiotz, J., Stoltze, P., Jacobsen, K.W. and Norskov, J.K. (1995) "Quantized conductance in atom-sized wires between two metals", *Phys. Rev. Lett.* **74**, 2147, Reply to comment on.
[23] Costa-Krämer, J.L., García, N., García-Mochales, P., Serena, P.A., Marqués, M.I. and Correia, A. (1997) "Conductance quantization in nanowires formed between micro and macroscopic metallic electrodes", *Phys. Rev. B* **55**, 5416–5424.
[24] Muller, C.J., van Ruitenbeek, J.M. and de Jongh, L.J. (1992) "Conductance and supercurrent discontinuities in atomic-scale metallic constrictions of variable width", *Phys. Rev. Lett.* **69**, 140–143.
[25] Krans, J.M., Muller, C.J., Yanson, I.K., Govaert, Th.C.M., Hesper, R. and van Ruitenbeek, J.M. (1993) "One-atom point contacts", *Phys. Rev. B* **48**, 14721–14724.
[26] Krans, J.M., van Ruitenbeek, J.M., Fisun, V.V., Yanson, I.K. and de Jongh, L.J. (1995) "The signature of conductance quantization in metallic point contacts", *Nature (Lond.)* **375**, 767–769.
[27] Costa-Krämer, J.L., García, N., García-Mochales, P. and Serena, P.A. (1995) "Nanowire formation in macroscopic metallic contacts: a universal property of metals", *Surf. Sci.* **342**, L1144–L1152, Erratum in *Surf. Sci.*, (**349**) (1996) L138.
[28] Rubio, G., Agraït, N. and Vieira, S. (1996) "Atomic-sized metallic contacts: mechanical properties and electronic transport", *Phys. Rev. Lett.* **76**, 2302–2305.
[29] Landman, U., Luedtke, W.D., Burnham, N.A. and Colton, R. (1990) "Atomistic mechanisms and dynamics of adhesion, nanoindentation, and fracture", *Science* **248**, 454–461.
[30] Scheer, E., Joyez, P., Esteve, D., Urbina, C. and Devoret, M.H. (1997) "Conduction channel transmissions of atomic-size aluminum contacts", *Phys. Rev. Lett.* **78**, 3535–3538.
[31] Scheer, E., Agraït, N., Cuevas, J.C., Levy Yeyati, A., Ludolph, B., Martín-Rodero, A., Rubio-Bollinger, G., van Ruitenbeek, J.M. and Urbina, C. (1998) "The signature of chemical valence in the electrical conduction through a single-atom contact", *Nature (Lond.)* **394**, 154–157.
[32] Díiaz, M., Costa-Krämer, J., Medina, E., Serena, P.A. and Hasmy, A. (2001) "Simulations and experiments of aluminum conductance histograms", *Nanotechnology* **12**, 118–120.
[33] Mehrez, H. and Ciraci, S. (1997) "Yielding and fracture mechanisms of nanowires", *Phys. Rev. B* **56**, 12632–12642.
[34] Buldum, A., Ciraci, S. and Batra, I.P. (1998) "Contact, nanoindentation, and sliding friction", *Phys. Rev. B* **57**, 2468–2476.
[35] Bratkovsky, A.M., Sutton, A.P. and Todorov, T.N. (1995) "Conditions for conductance quantization in realistic models of atomic-scale metallic contacts", *Phys. Rev. B* **52**, 5036–5051.
[36] Sorensen, M.R., Brandbyge, M. and Jacobsen, K.W. (1998) "Mechanical deformation of atomic-scale metallic contacts: structure and mechanisms", *Phys. Rev. B* **57**, 3283–3294.
[37] Haftel, M.I. (1993) "Surface reconstruction of platinum and gold and the embedded-atom model", *Phys. Rev. B* **48**, 2611–2622.
[38] García-Martín, A., Torres, J.A. and Sáenz, J.J. (1996) "Finite size corrections to the conductance of ballistic wires", *Phys. Rev. B* **54**, 13448–13451.
[39] Brack, M. (1993) "The physics of simple metal clusters: self-consistent jellium model and semiclassical approaches", *Rev. Mod. Phys.* **65**, 677–732.
[40] Yannouleas, C., Bogachek, E.N. and Landman, U. (1998) "Energetics, forces, and quantized conductance in jellium-modeled metallic contacts", *Phys. Rev. B* **57**, 4872–4882.

[41] Yanson, A.I., Yanson, I.K. and van Ruitenbeek, J.M. (1999) "Observation of shell structure in sodium nanowires", *Nature (Lond.)* **400**, 144.
[42] Yanson, A.I. (2000) "Supershell structure in alkali metal nanowires", *Phys. Rev. Lett.* **84**, 5832–5835.
[43] Díaz, M., Costa-Krämer, J.L., Medina, E., Hasmy, A. and Serena, P.A. (2003) "Evidence of shell structures in Au nanowires at room temperatures", *Nanotechnology* **14**, 113–116.
[44] Gulseren, O., Ercolessi, F. and Tosatti, E. (1998) "Noncrystalline structures of ultrathin unsupported nanowires", *Phys. Rev. Lett.* **80**, 3775–3778.
[45] Tosatti, E., Prestipino, S., Kostlmeier, S., Dal Corso, A. and Di Tolla, F. (2001) "String tension and stability of magic tip-suspended nanowires", *Science* **291**, 288.
[46] Yanson, A.I., Yanson, I.K. and van Ruitenbeek, J.M. (2001) "Crossover from electronic to atomic shell structure in alkali metal nanowires", *Phys. Rev. Lett.* **87**, 216805.
[47] Fiorentini, V., Methfessel, M. and Scheffler, M. (1993) "Reconstruction mechanism of fcc transition metal (0 0 1) surfaces", *Phys. Rev. Lett.* **71**, 1051–1054.
[48] Haftel, M.I. and Rosen, M. (1995) "Molecular-dynamics description of early film deposition of Au on Ag(1 1 0)", *Phys. Rev. B* **51**, 4426–4434.
[49] Shchukin, V.A. and Bimberg, D. (1999) "Spontaneous ordering of nanostructures on crystal surfaces", *Rev. Mod. Phys.* **71**, 1125–1171.
[50] Mitome, M., Takayanagi, K. and Tanishiro, Y. (1990) "Commensurate reconstruction on a (0 0 1) facet of a gold particle", *Phys. Rev. B* **42**, 7238–7241.
[51] Nieminen, J.A. (1995) "Temperature dependence of surface reconstruction of Au on Pd(1 1 0)", *Phys. Rev. Lett.* **74**, 3856–3859.
[52] Kondo, Y., Ru, Q. and Takayanagi, K. (1999) "Thickness induced structural phase transition of gold nanofilms", *Phys. Rev. Lett.* **82**, 751–754.
[53] Ohnishi, H., Kondo, Y. and Takayanagi, K. (1998) "Quantized conductance through individual rows of suspended gold atoms", *Nature (Lond.)* **395**, 780–783.
[54] Rodrigues, V., Fuhrer, T. and Vgarte, D. (2000) "Signature of atomic structure in the quantum conductance of gold nanowires", *Phys. Rev. Lett.* **85**, 4124–4127.